Supplementary Information for

Paul Trapping of Charged Particles in Aqueous Solution

Weihua Guan,[1] Sony Joseph,[2] Jae Hyun Park,[2] Predrag S. Krstić,[2] and Mark A. Reed[1,3,*]

[1]*Department of Electrical Engineering,*

Yale University, New Haven, Connecticut 06520

[2]*Physics Division, Oak Ridge National Laboratory, Oak Ridge, Tennessee 37831*

[3]*Applied Physics, Yale University, New Haven, Connecticut 06520*

[*] Electronic Address: mark.reed@yale.edu

CONTENTS

S1. DEVICE FABRICATION

Our planar quadrupole trapping devices are fabricated on a SiO_2/Si wafer (Fig. S1a). The insulating SiO_2 layer has a thickness of 3 μm which is thermally grown. LOR 5A resist (Microchem Corp) is spined on the substrate at a speed of 3000 rmp for 1 min, followed by baking at 175 °C for 5 min on the hotplate. Another layer of positive photoresist S1808 (Shipley) is then spun on top of the baked LOR. Then a standard UV lithography and developing process is applied to pattern the bi-layer structure. 20-nm-thick Cr and 300-nm-thick Au is e-beam evaporated at the speed of 3 $\mathring{A}/s$. The whole wafer is thereafter immersed into the N-Methylpyrrolidone (NMP) solution heated at 60°C to remove the bi-layer photoresist. Finally, the wafer is diced and is ready to be integrated with the microfluidic chamber. The microfluidic chamber is formed by poly(dimethylsiloxane) (PDMS) using SU-8 as a molding master (Fig. S1c and d). The detailed protocols can be found in ref. [1]. Oxygen plasma treatment was used to permanently bond the PDMS to the device surface and form an anti-evaporation microfluidic channel(Fig. S1e). An inlet and an outlet were punched through before assembling(Fig. S1f). Once the device was assembled, it could be repeatedly used for a long time.

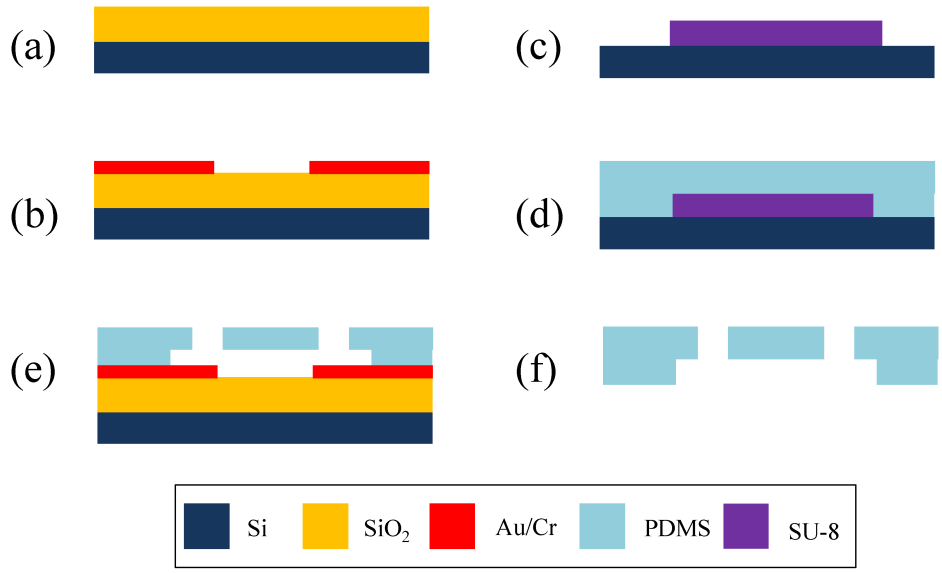

Figure S1. Schematic device fabrication flow

S2. VIDEO PROCESSING METHOD

We use a particle tracking algorithm that has been described in detail elsewhere [2] to extract the motion fluctuations. The videos are taken by a high-sensitivity digital CCD camera (Olympus DP70) with the highest shutter speed as fast as 1/44000 s. Videos are decomposed into frame sequences using the software VirtualDub (`http://www.virtualdub.org/`). The particle tracking is then carried out in NIH ImageJ platform (`http://rsb.info.nih.gov/ij/`) with a particle tracking plugin tool developed by G. Levy (`https://weeman.inf.ethz.ch/ParticleTracker/`). Fig. S2 illustrates the trajectory extraction process.

However, video based position extraction method does not measure the instantaneous particle position and has a problem of 'motion blur', which results from time-averaging a signal over a finite integration time (shuttle time or acquisition time) [3]. This will lead to the underestimation of the real variance. Wong *et al.* showed both theoretically and experimentally that the relation between the measured variance $Var(X_m)$ and the real variance $Var(X_r)$ can be linked by motion blur correction function $S(\alpha)$ [3], $Var(X_r) = Var(X_m)/S(\alpha)$, where $S(\alpha) = \frac{2}{\alpha} - \frac{2}{\alpha^2}(1 - e^{-\alpha})$, and α is a dimensionless parameter, defined by expressing the exposure time W in unit of the trap relaxation time τ, i.e. $\alpha = W/\tau$.

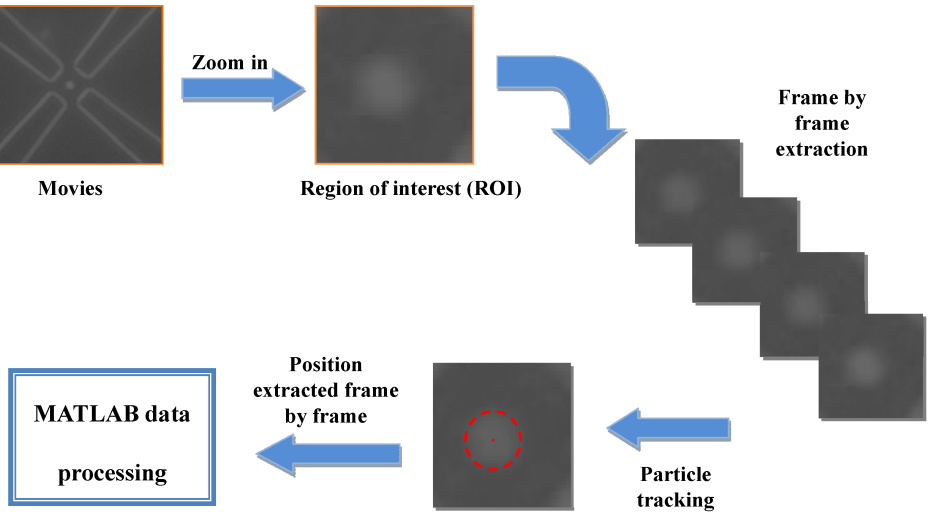

Figure S2. Illustration of trajectory extraction method

As for the position variance extraction experiments, we set the shutter speed as 1/80 s and used a 100× objective, leading to an on-screen magnification of 125 nm/pixel. The recording

frame rate is 8 fps. We estimate the relaxation time in the experiment as $\tau = \xi/k \sim 1ms$ (where $\xi = 6\pi\eta r$, the Stokes' drag coefficient). As a result, the motion blur correction function value $S(\alpha)|_{\alpha=12.5} = 0.1472$. Therefore, the real variance $Var(X_r)$ is corrected as, $Var(X_r) = 6.79 \times Var(X_m)$, or in terms of standard deviation, $Std(X_r) = 2.6 \times Std(X_m)$

S3. SOLUTION PREPARATION

The solution used in the experiment was prepared by the following steps:

(1) The beads were firstly diluted to a density of $\sim 10^6$ particle/mL by deionized (DI) water (milli-Q grade, resistivity 18 $M\Omega \cdot cm$), in order to eliminate the particle-particle interactions during the experiment.

(2) In order to thoroughly remove the residual ions from the stock solution, the beads prepared in step 1 were washed five times in DI water by centrifuging the beads in a 10 mL tube at 13500 G for 10 min, re-suspending in DI water each time.

The prepared solution in the 10 mL tube was extracted and then pumped into the microfluidic chamber. The conductivity of the fresh suspension solution in the 10 mL tube (exposed to air) is measured as 0.1 $\mu S/cm$ (EC 215 Multi-range Conductivity Meter, Hanna Instruments) and this slowly goes up to maximum 2.0 $\mu S/cm$ during the course of an experiment (due to the absorption of ambient gas). This measured conductivity variation sets the lower and upper bound for the solution inside the microfluidic chamber. In fact, since the microfluidic channels are not directly exposed to air, little change of the solution conductivity inside the trap chamber is expected. Since the solution conductivity directly affects the effective charge of the particle (see Section S4), long-term measurements were carried out on a single trapped particle to investigate the drift of solution conductivity. We find that we can stably trap particles for a minimum of 4 hours (we did not explore longer), and over this time the trap stiffness ($k = k_B T/\delta^2$) only changed by $< 3\%$ (Fig. S3), indicating a stable solution conductivity during the 4-hour period.

S4. EFFECT OF SOLUTION CONDUCTIVITY

Maintaining a low solution conductivity is critical to observe the Paul trapping effects (instead of DEP effects) for our current devices. Notice that the charge we used in the

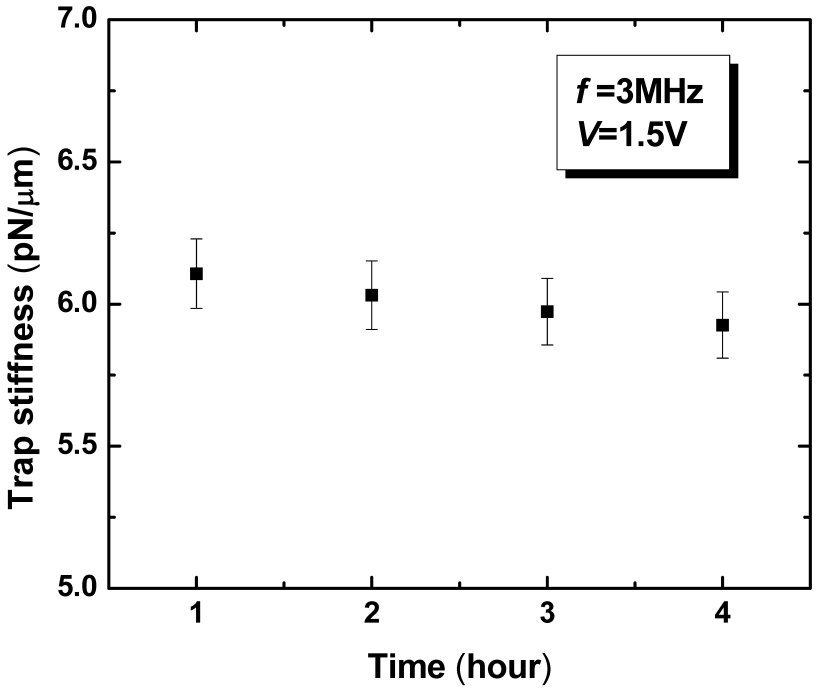

Figure S3. Long-term trap stiffness for a single trapped bead (particle radius 491 nm and device size R_0=4 μm).

derivations in the main text is the effective charge rather than the bare charge. A charged surface in contact with a conductive liquid creates an induced electric double layer (EDL). A significant fraction of the particle's charge is neutralized by the strongly bounded counterions in the Stern layer. The charged particle plus the thin Stern layer is further screened by diffusive counterions within a characteristic Debye length λ_D. To determine the effective charge Q_{eff}, we look at the motion of charged particles, which is induced by electrostatic forces, friction, and electrophoretic retardation forces. Among them, the electrophoretic retardation force originates from the delayed response of the surrounding ionic atmosphere to the motion of a charged particle. The electrophoretic mobility including this retardation effect can be described by Henry's formula [4],

$$\mu_E = \frac{2}{3}\frac{\varepsilon\zeta}{\eta} f(\alpha) \tag{S1}$$

where $\alpha = a/\lambda_D$ is the ratio of particle radius to the Debye length of the electrolyte solution, ε is the dielectric constant of the electrolyte, ζ is the zeta-potential, and η is viscosity of the solution. Ohshima *et al.* [5] showed that $f(\alpha)$ is a monotonic increasing function that

varies from 1 to 3/2. Since ζ-potential can be expressed in Debye-Hückel form [6],

$$\zeta = \frac{Q_{bare}}{4\pi\varepsilon a\left(1 + a/\lambda_D\right)} \tag{S2}$$

where Q_{bare} is the bare charge of particle. The electrophoretic mobility μ_E can be rewritten as,

$$\mu_E = \frac{Q_{bare}}{6\pi\eta a\left(1 + a/\lambda_D\right)} f\left(\frac{a}{\lambda_D}\right) \tag{S3}$$

The effective charge of particle can thus be estimated as,

$$Q_{eff} = \frac{f\left(a/\lambda_D\right)}{\left(1 + a/\lambda_D\right)} Q_{bare} \tag{S4}$$

At a high ionic concentration c, the Debye length ($\lambda_D \sim c^{-1/2}$) becomes very small, as a result, $a/\lambda_D \gg 1$ and $f\left(a/\lambda_D\right) \to 3/2$. Therefore, $Q_{eff} \approx \frac{3}{2}\frac{\lambda_D}{a} Q_{bare} \ll Q_{bare}$. The effective charge is greatly reduced in salt solutions. However, a significant amount of charge of the particle is required for Paul trap to function (Paul trap would not work with neutral particles). For most DEP trapping experiments reported, high salt concentrations were added to adjust the conductivity of the suspension medium [7–11]. Therefore the Paul trap effects can not be seen easily in these experiments. In contrast, it is easy to see that $Q_{eff} \to Q_{bare}$ when $a \to 0$ and/or $\lambda_D \to \infty$. This will happen for ultrasmall particles or very low ionic concentrations.

S5. MOVIE ILLUSTRATIONS

The affiliated video shows typical dynamics for four basic operations.

(i) Trapping with small fluctuations.

(ii) Trapping with large fluctuations.

(iii) Unstable trapping region, ejection.

(iv) Resuming trapping.

Table SI summarizes the working conditions for each part of the video. It is worth noting that for the two particles in part (iv), one particle is leaving while the other is trapped. This is believed to be due to the inter-particle coulomb repulsion. We observe in the experiment that the trapping mostly occurred for single beads, though up to 4 beads trapped simultaneously are also occasionally observed.

TABLE SI. Working parameters for each part in the video [a,b]

Video part	RF voltage (V)	DC voltage (V)	Frequency (MHz)	b	q	a
i	1.72	0	3	1.89	0.2727	0
ii	0.92	0	3	1.89	0.1458	0
iii	0.68	0	3	1.89	0.1078	0
iv	1.84	0	3	1.89	0.2917	0

[a] The device size is $2R_0$=7.4 μm, bead radius is r_p=490 nm.

[b] b, q and a parameters are calculated by using $Q/\Gamma M = 4.77 \times 10^{-6}$ e/amu.

S6. CALCULATION OF THE ELECTRIC POTENTIAL FOR THE REAL PLANAR DEVICE GEOMETRY

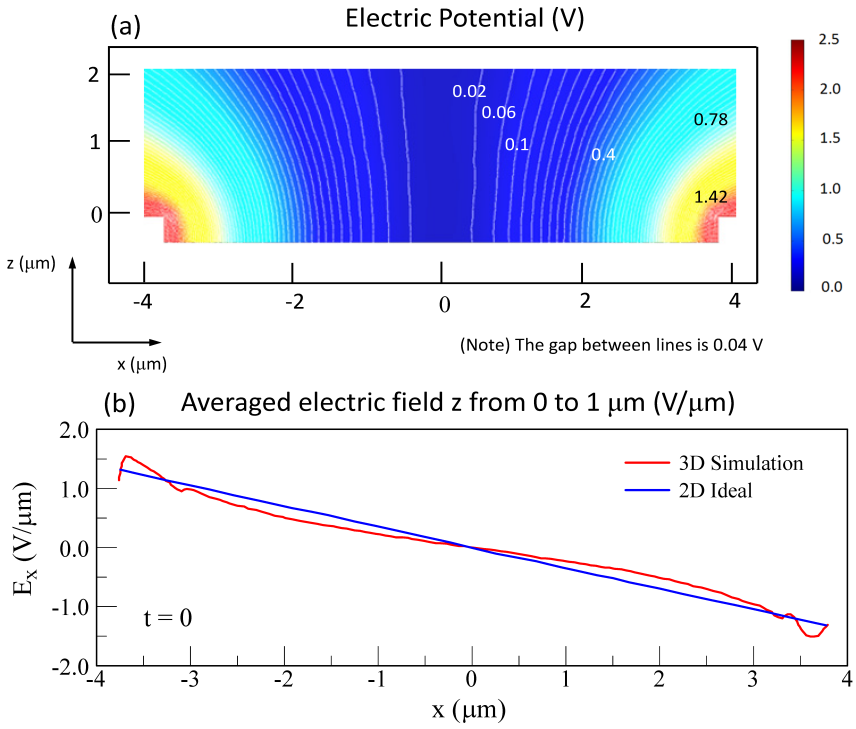

Figure S4. (a) The electric potential distribution in $x-z$ plane calculated for the real 3D geometry. (b) Comparison of the x-component potential for the real device with finite height (averaged over z from 0 to 1 μm) and an ideal 2D device at one instant of time (t=0).

We numerically calculated (using COMSOL software package, `http://www.comsol.com`,

COMSOL Multiphysics Ouick Start and Quick Reference, COMSOL LAB.)) a 3D potential distribution in the trap for an AC potential of 5 Vpp (peak to peak voltage) on the electrodes for the device geometry extracted from a SEM image. Fig. S4(a) shows the potential profile in a cross section ($x-z$ plane) for this realistic geometry. From the result it is seen that as long as the spherical particle remains within the height of the electrodes, it is close to an ideal 2D trap. Above the electrodes, the potential changes as if the device size is increased. The lines around z= 2 μm (chamber height 2.5 μm) shows where along the z axis the microfluidic chamber walls restrict the motion of the particle. Fig. S4(b) is a comparison of the x-component potential for the real device with finite height (averaged over z from 0 to 1 μm) and an ideal 2D device at one instant of time (t=0).

S7. CONSIDERATION OF DEP TRAPPING MECHANISM

S7.1. Theoretical calculation of DEP impact on stability diagram

Besides the direct interaction of the particle's net charges and the electric field (Paul trap), there are also interactions between the particle's polarizability and the electric field. Here we consider the impact of dielectrophoretic (DEP) forces on the $q-a$ stability diagram. The dimensionless form of the equation of motion in x-direction of a charged particle of radius a in the Paul trap defined by parameters a and q (Eq. [3] of the main text), with damping defined by factor b, in presence of DEP forces, can be written as

$$\frac{d^2x}{d\tau^2}+b\frac{dx}{d\tau}+[a+\alpha_m K(\Omega)(aU+qV)-2q(1+2\alpha_m K(\Omega)U)\cos 2\tau+\alpha_m K(\Omega)qV\cos 4\tau]=0 \quad \text{(S5)}$$

where $\alpha_m = 4\pi a^3\varepsilon_m/QR_0^2$, and $K(\Omega)$ is the Clausius-Mossotti factor. It is easy to see that the expression above is reduced to homogeneous part of Eq. [3] in the main text when $K(\Omega)$=0 (without DEP effect).

We consider two extreme cases of DEP, the one with positive $K(\Omega)$=1 (positive DEP, pDEP), and the one with $K(\Omega) = -1/2$ (negative DEP, nDEP). We treat the above equation numerically, and find that the effect of DEP is significant only for extremely small q and a factors of Paul trap (for example, small charges of the particle). The stability diagram (solid line) from Fig. 3 in the main text is shown in Fig. S5 by solid blue line. DEP corrections only contribute a small perturbation near the $q-a$ origin ($q < 0.01$), far below the region

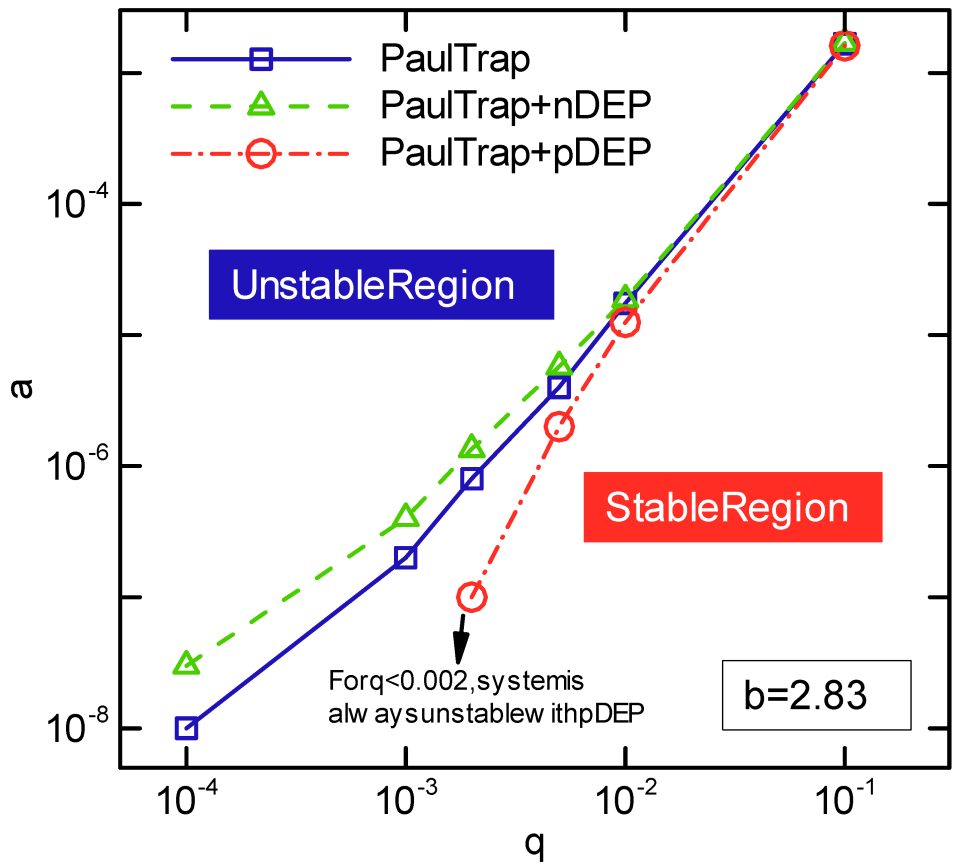

Figure S5. Magnified $q - a$ stability diagram near origin

of experimental interest ($q > 0.1$). The impact of DEP on the stability is negligible for the parameters of the Paul trap used in the present study.

S7.2. Particle size dependence experiment

The time averaged DEP force can be estimated as $\langle F_{dep} \rangle = \pi \varepsilon_m a^3 Re[K(\omega)] \nabla E_0^2(\vec{r})$. It scales with the particle volume ($\sim a^3$). Therefore, the DEP trap stiffness will decrease as a function of particle volume. On the contrary, time averaged Paul trap force can be estimated by $\langle F_{pt} \rangle = Q^2 \nabla E_0^2(\vec{r})/(4M\Omega^2(1 + (\xi/M\Omega)^2))$. Instead of a simple dependence on the particle volume, the Paul trap stiffness depends on the charge Q and mass M in a complex way. Measurements of the trap stiffness as a function of the particle size reveal whether the trapping mechanism in our experiment is dominated by DEP effect or Paul trap effect.

We used the polystyrene beads with radius ranging from 240 nm to 1.5 μm. All of these beads are surface functionalized with carboxylate surface groups. Their sizes are well characterized while the surface charge density is undetermined. The surface charges do not necessarily scale with the surface area of the particle. The suspension solution is thoroughly washed using the same procedure described above. All the trap stiffness are extracted under the condition of V=1.5 V, U= 0 V, and f=2.5 MHz, using the device with the same size (8 μm between electrode tips). Fig. S6 shows the measured trap stiffness as a function of the particle radius. As is shown, the trap stiffness does not scale with the particle volume ($\sim a^3$). In fact, when the particle radius reduces from 0.491 μm to 0.24 μm, the trap stiffness increases from 4 pN/μm to 15.2 pN/μm. This strongly proves that the trapping mechanism is not due to the DEP effect, as one would expect a decrease of trap stiffness when decreasing the particle size. We note that the irregular dependence of the trap stiffness on the particle radius in Fig. S6 comes from the irregular Q/M ratio for different particles.

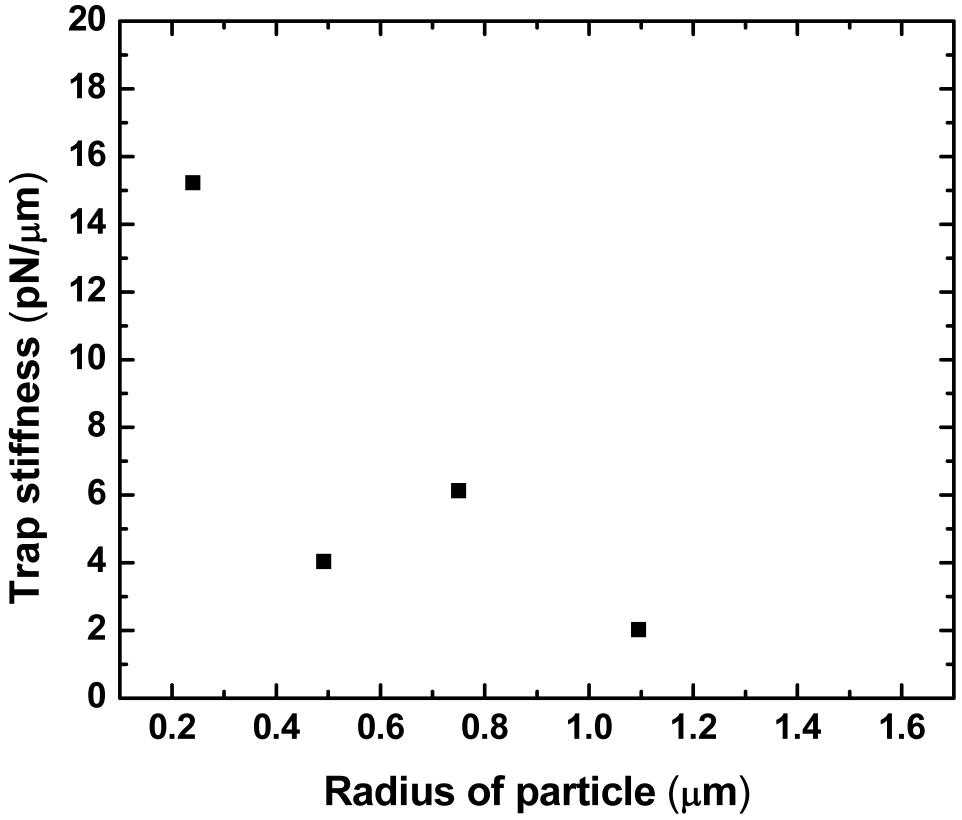

Figure S6. Trap stiffness as a function of the particle radius

S7.3. Frequency dependence experiment

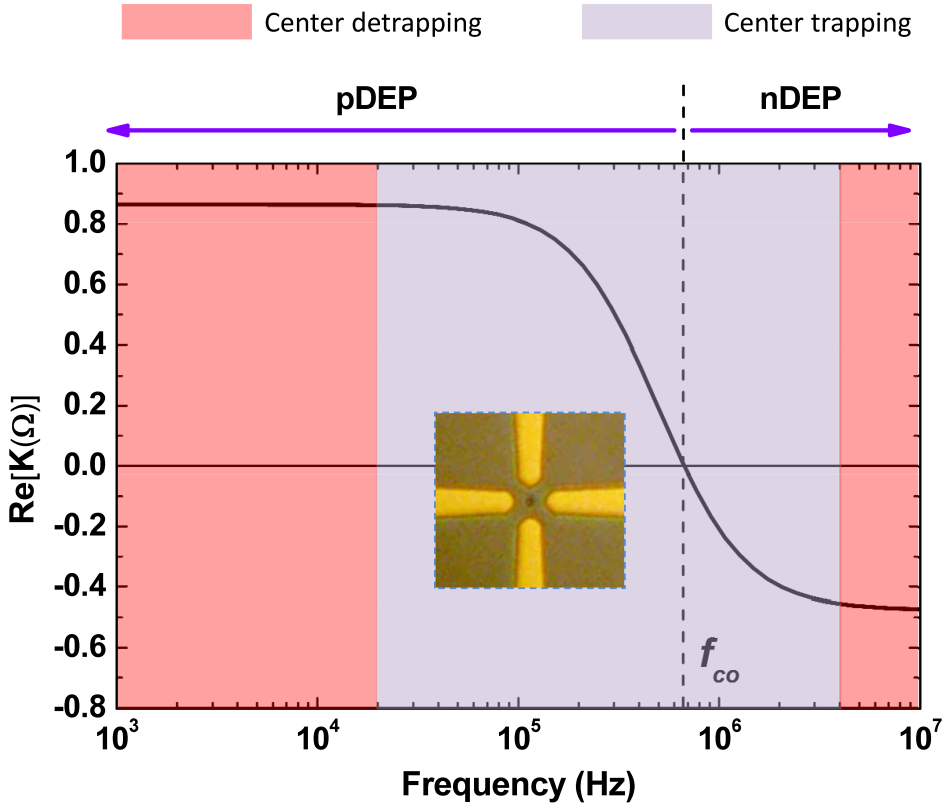

Figure S7. Particle can be trapped in the center of the device (local electric field minima) even when the operation frequency is in the positive DEP region.

Both the Paul trap and DEP effects are frequency dependent, but in a very different way. For DEP effect, the sign associated with the real part of Clausius-Mossotti (CM) factor (Re[K(ω)], which is frequency dependent) dictates the behavior of the particle [12]. For Re[K(ω)]>0, particles will be directed toward a local electric field maxima (positive DEP, pDEP), while for Re[K(ω)]<0, particle is attracted to a local electric field minima (negative DEP, nDEP). In other word, nDEP drags the particle to the center of the device while pDEP pushes the particle out of the device center. The frequency that produces a change from pDEP to nDEP is referred to as the crossover frequency f_{co} (Hz) and is given by $(1/2\pi)[(\sigma_p - \sigma_m)(\sigma_p + 2\sigma_m)/(\epsilon_m - \epsilon_p)(\epsilon_p + 2\epsilon_m)]^{1/2}$, where σ and ϵ are the conductivity and permittivity, respectively, with p and m denoting the particle and medium.Note that this crossover frequency theory is well supported by experiments [10]. For a Paul trap, the

particle confinement to the center of the trap is determined by if the $a = 4QU/MR_0^2\Omega^2$and $q = 2QV/MR_0^2\Omega^2$ parameters are within the stability region or not. It is because of this frequency dependence that we can experimentally map out the stability diagram for Paul trap (Figure 4a in main text). DEP trap would not have the (q,a) stability boundary. To more convincingly rule out the DEP effect as the trapping mechanism in the considered region of the trap parameters, we carried out the following frequency dependence experiment. Using the suspension of the low conductivity solution (prepared by the same procedure described in Section S3), we measured the solution conductivity as $\sigma_m = 2\mu S/cm$. $\sigma_p = 40\mu S/cm$(by taking into account the surface conductance). With $\varepsilon_p = 2.55\varepsilon_0$ and $\varepsilon_m = 78\varepsilon_0$, we calculate the crossover frequency frequency as f_{co}=670 KHz. Therefore, the particle will undergo a pDEP force and should be kicked out of the device center when f_{co} <670 KHz. In our experiment, the bead can be trapped in the center of the device even when the frequency is ramped down to 20 KHz due to Paul trapping (Fig. S7). Therefore, DEP effect is not a dominant mechanism. It is the Coulomb interaction of the particle charge and the Paul trap quadrupole oscillating field, together with the damping (friction) forces of the water that confine the particle toward the trap center even when the particle is subject to a pDEP force, which tends to push the particle out of the center.

S8. ANOTHER SET OF LINEAR FITTING DATA

Fig. S8 shows another independent set of the data by examining another single trapped particle when frequency f=3 MHz. A linear dependence of the rms fluctuation on $1/V$ is clearly seen. The reduced χ^2 value calculated from the linear fit in Fig. S8 is 0.26.

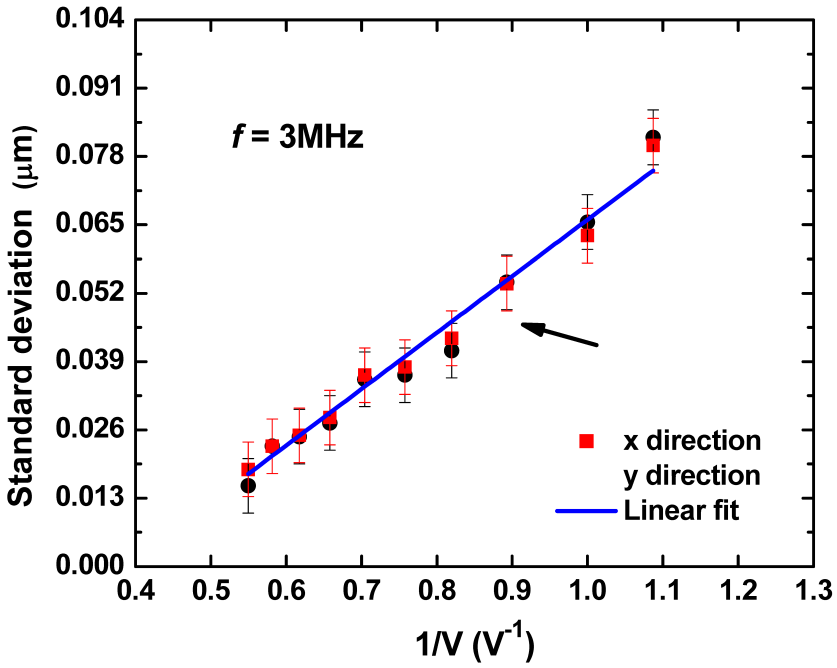

Figure S8. Dependence of the standard deviation of position fluctuations of a trapped bead on AC voltage at fixed frequency (3 MHz) for another independent experiment.

[S1] Duffy, D. C, McDonald, J. C, Schueller, O. J. A, & Whitesides, G. M. (1998) Rapid prototyping of microfluidic systems in poly(dimethylsiloxane). *Analytical Chemistry* **70**, 4974–4984.

[S2] Sbalzarini, I. F & Koumoutsakos, P. (2005) Feature point tracking and trajectory analysis for video imaging in cell biology. *Journal of Structural Biology* **151**, 182–195.

[S3] Wong, W. P & Halvorsen, K. (2006) The effect of integration time on fluctuation measurements: calibrating an optical trap in the presence of motion blur. *Optics Express* **14**, 12517–12531.

[S4] Henry, D. C. (1931) The cataphoresis of suspended particles. part i. the equation of cataphoresis. *Proceedings of the Royal Society of London. Series A* **133**, 106–129.

[S5] Ohshima, H, Healy, T. W, & White, L. R. (1983) Approximate analytic expressions for the electrophoretic mobility of spherical colloidal particles and the conductivity of their dilute suspensions. *Journal of the Chemical Society, Faraday Transactions 2* **79**, 1613–1628.

[S6] Palberg, Mnch, Bitzer, Piazza, & Bellini. (1995) Freezing transition for colloids with adjustable charge: A test of charge renormalization. *Physical Review Letters* **74**, 4555–4558.

[S7] Fiedler, S, Shirley, S. G, Schnelle, T, & Fuhr, G. (1998) Dielectrophoretic sorting of particles and cells in a microsystem. *Analytical chemistry* **70**, 1909–1915.

[S8] Muller, T, Gerardino, A, Schnelle, T, Shirley, S. G, Bordoni, F, DeGasperis, G, Leoni, R, & Fuhr, G. (1996) Trapping of micrometre and sub-micrometre particles by high-frequency electric fields and hydrodynamic forces. *Journal of Physics D: Applied Physics* **29**, 340–349.

[S9] Hughes, M. P & Morgan, H. (1998) Dielectrophoretic trapping of single sub-micrometre scale bioparticles. *Journal of Physics D: Applied Physics* **31**, 2205–2210.

[S10] Green, N. G & Morgan, H. (1999) Dielectrophoresis of submicrometer latex spheres. 1. experimental results. *Journal of Physical Chemistry B* **103**, 41–50.

[S11] Voldman, J, Braff, R. A, Toner, M, Gray, M. L, & Schmidt, M. A. (2001) Holding forces of single-particle dielectrophoretic traps. *Biophysical Journal* **80**, 531–541.

[S12] Pohl, H. A. (1978) *Dielectrophoresis: the behavior of neutral matter in nonuniform electric fields*. (Cambridge University Press.).